Springer

KSME

Journal of Mechanical Science and Technology 31 (4) (2017) 1877~1884
www.springerlink.com/content/1738-494x(Print)/1976-3824(Online)
DOI 10.1007/s12206-017-0335-6

Surface quality prediction model of nano-composite ceramics in ultrasonic vibration-assisted ELID mirror grinding †

Bo Zhao, Fan Chen*, Xiao-feng Jia, Chong-yang Zhao and Xiao-bo Wang

School of Mechanics and Power Engineering, Henan Polytechnic University, Jiaozuo, 454003, China

(Manuscript Received September 5, 2016; Revised November 3, 2016; Accepted December 13, 2016)

Abstract

Ultrasonic vibration-assisted Electrolytic in-process dressing (ELID) grinding is a highly efficient and highly precise machining method. The surface quality prediction model in ultrasonic vibration-assisted ELID mirror grinding was studied. First, the interaction between grits and workpiece surface was analyzed according to kinematic mechanics, and the surface roughness model was developed. The variations in surface roughness under different parameters was subsequently calculated and analyzed by MATLAB. Results indicate that compared with the ordinary ELID grinding, ultrasonic vibration-assisted ELID grinding is superior, because it has more stable and better surface quality and has an improved range of ductile machining.

Keywords: Prediction model; Surface quality; Nano-composite ceramics; Ultrasonic; Electrolytic in process dressing; Mirror grinding

1. Introduction

Nanocomposite ceramics, micron, or submicron matrix grains coexisting with nano-strengthening phase particles, has been studied for the last 10 years. Nanoparticles are distributed in the matrix grain materials, thereby enhancing the grain boundary strength and greatly improving the mechanical performance and reliability of materials; these effects improve the resiliency of brittle ceramics and provide a foundation for the widespread use of structural components [1-3]. Despite these enhancements, nanocomposite ceramics still exhibit low durability, and its hardness and sensitivity to defects remains high. Thus, nanocomposite ceramics have limited applications, because of their high finishing costs. In addition, it receives damages during the finishing process. Therefore, developing a cost-effective machining technique for nanocomposite ceramics is important. A cost-effective technique can have various applications in national economy and defense. In this regard, researchers have examined many ultraprecise machining methods, such as pre-stretched machining, Electrolytic in-process dressing (ELID) grinding, magnetic abrasive polishing, and ultrasonic vibration-assisted machining [4-7]. Ultrasonic vibration-assisted ELID mirror grinding is a combination of ELID grinding and ultrasonic vibration-assisted machining and is a new machining technique that can improve surface quality and grinding efficiency [8-11].

*Corresponding author. Tel.: +86 391 3987501, Fax.: +86 391 3987512
E-mail address: kuailetianshi028@163.com
† Recommended by Editor Haedo Jeong

In mirror grinding, the grinding depth is usually smaller than the critical ductile depth. In addition, the removal of nanocomposite ceramics is mainly performed in ductile removal mode. This technique is similar to cutting metals in such a manner that the material is removed by localized shear chips from sliding friction, to plowing, and finally to chip formation. In mechanical drawing, R_a is the arithmetical mean deviation of the profile, and R_z is the maximum height of the profile. R_a and R_z are usually used as general parameters to evaluate the surface structure. Under ideal conditions wherein the workpiece material is a rigid plastic, abrasive on grinding wheel is not worn, grinding depth is constant, and other conditions are unchanged, $2R_a = R_z$. In this equation, R_z can amplify the change of R_a. R_z roughness not only reflect the variety of Ra, but also verify the correctness of the theoretical analysis. In such conditions, the generating interaction between grits and workpiece surface can be analyzed on the basis of kinematic mechanics, and the surface roughness (R_z) model can be developed. Then variations in surface roughness (R_z) under different parameters can be predicted using a mathematical model, which is significant in both theoretical and practical aspects.

2. Development of the surface roughness model

2.1 Additional effect of ultrasonic vibration on single grit

Supposing that the diamond grains are rigid spheres with uniform radius (r_s), and the internal grinding with ultrasonic assistance in the z direction, as shown in Fig. 1, is perpendicu-

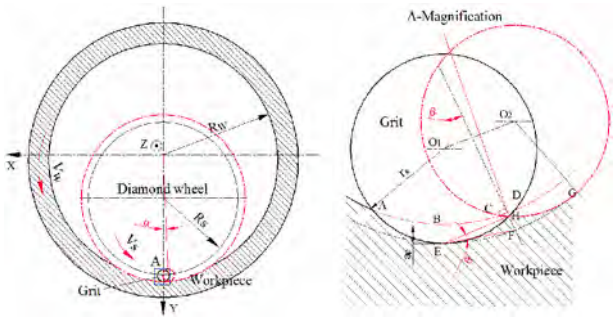

Fig. 1. Cross section of wheel-workpiece contact area.

lar to the axes of both the grinding wheel and workpiece, the height of the grinding trace on the workpiece surface (FH) can be regarded as the maximum height of the profile (R_z'), which is derived from differential geometry.

$$R_z' = FH = \overline{EF} \cdot \sin\theta \approx \overset{\frown}{\mathrm{EF}} \cdot \sin\theta \approx \frac{1}{2}\overset{\frown}{\mathrm{EFG}} \cdot \sin\theta \,, \tag{1}$$

where $\overset{\frown}{\mathrm{EFG}}$ is equal to the arc length on the workpiece when the grinding wheel turns two adjacent grits internal spacing (Δ).

$$\overset{\frown}{\mathrm{EFG}} = V \cdot t \tag{2}$$

and

$$t = \frac{\Delta}{V_s} \,. \tag{3}$$

Assuming that the abrasive on the grinding wheel are uniformly distributed, we can obtain the relationship between the volume fraction (V_g) and Δ on the grinding wheel according to the different geometric expressions of the volume of the abrasive on the wheel.

$$\frac{4}{3}\pi\left(\frac{d_{g_{avg}}}{2}\right)^3 = V_g \cdot \Delta^3 \,. \tag{4}$$

Thus, Δ can be shown as

$$\Delta = \sqrt[3]{\frac{\pi}{6V_g}} \cdot d_{g_{avg}} \,, \tag{5}$$

where d_{gavg} is the average diameter of the abrasive particle.

In ultrasonic vibration-assisted ELID circular grinding, the speed of the single diamond grit can be expressed as

$$\begin{aligned} V &= \sqrt{d_x^{\,2} + d_y^{\,2} + d_z^{\,2}} \\ &= \sqrt{\begin{aligned}&[(R_w + a_p)\cdot(\sin\alpha)]^2 + [(R_w + a_p)\cdot\cos\alpha]^2 \\ &+[\frac{R_w \cdot f_a}{V_s - V_w} + 2\cdot A\cdot\pi\cdot f\cdot\frac{R_w}{V_s - V_w}\cos(2\cdot\pi\cdot f\cdot\frac{R_w\cdot\alpha}{V_s - V_w})]^2\end{aligned}} \end{aligned} \tag{6}$$

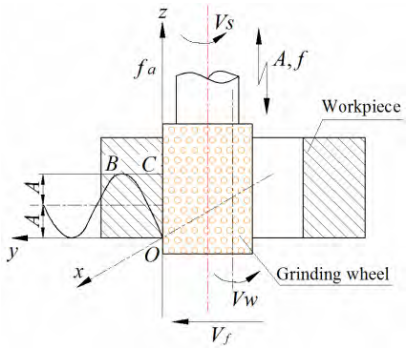

Fig. 2. Sketch of geometrically generating interaction between the grinding wheel and the workpiece.

where f_a is the axial feed velocity, f is the ultrasonic frequency, A is the ultrasonic amplitude, and α is the angle of the abrasive corresponding to the corner of the workpiece.

When α is extremely small, we can assume that $\sin\alpha$ is ~0 and $\cos\alpha$ is ~1 such that the speed of the single diamond grit can be rewritten as

$$V = \sqrt{(R_w + a_p)^2 + [\frac{R_w \cdot f_a}{V_s - V_w} + 2\cdot A\cdot\pi\cdot f\cdot\frac{R_w}{V_s - V_w}]^2} \,. \tag{7}$$

In Fig. 1, when the angle (θ) is extremely small, $\sin\theta$ can be obtained by constructing a geometric model.

$$\sin\theta = 2\sqrt{2a_p(\frac{1}{R_s} - \frac{1}{R_w})} \,. \tag{8}$$

According to Eqs. (1)-(8), the surface roughness (R_z') for a grain can be expressed as

$$R_z' = \sqrt{2}\cdot\sqrt[3]{\frac{\pi}{6V_g}}\cdot\frac{d_{g_{avg}}}{V_s}\cdot\sqrt{\begin{aligned}&a_p\cdot(\frac{R_w - R_s}{R_s\cdot R_w})\cdot\{(R_w + a_p)^2 \\ &+[\frac{R_w\cdot f_a}{V_s - V_w} + 2\cdot A\cdot\pi\cdot f\cdot\frac{R_w}{V_s - V_w}]^2\}\end{aligned}} \,. \tag{9}$$

2.2 Additional effects of ultrasonic vibration on adjacent abrasive grits

In ultrasonic vibration-assisted ELID grinding processing, the geometrically generating interaction between the grits and workpiece surface is different from that in the ordinary ELID grinding because of the axial ultrasonic vibration of the grinding wheel, as shown in Fig. 2.

As seen in Fig. 2, when the particle size is disregarded, a grain on an arbitrary point of the grinding wheel is considered as a particle, and its displacement in all directions can be expressed as

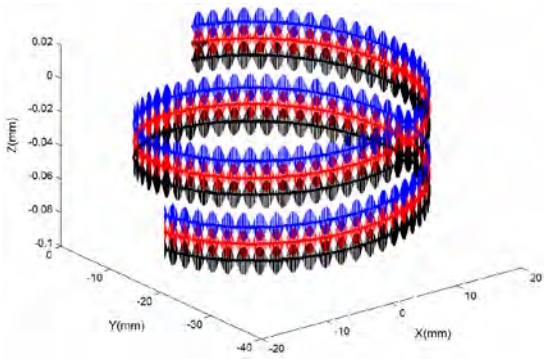

Fig. 3. Sketch of the movement track of three adjacent abrasive particles in ordinary and ultrasonic vibration-assisted ELID grinding.

$$\begin{cases} l_x = (V_S - V_W)\cdot t \\ l_y = V_f \cdot t \\ l_z = f_a \cdot t + \mathrm{A}\cdot\sin(2\pi\cdot f\cdot t+\phi) \end{cases}, \tag{10}$$

where V_f is the feed speed of the work table and φ is the initial angle of ultrasonic vibration. Ordinary ELID grinding is used when the ultrasonic amplitude (A) is 0.

According to the movement equation under U-ELID grinding and ELID grinding, the difference of the three adjacent grits in ordinary from ultrasonic vibration-assisted ELID grinding is shown in Fig. 3.

In ordinary ELID grinding, the nonintervention conditions of the three adjacent abrasive particles form helical lines, and the machined surface of the workpiece is attributed mostly to the continuous cutting of the abrasive particles. However, in ultrasonic vibration-assisted ELID grinding, the additional ultrasonic vibration affects the workpiece. The movement track distribution of a single abrasive grain forms a sinusoid or cosine curve resembling a helix, which results in elliptical cutting traces in the cross section and overlapping of adjacent particle trajectories, thereby forming the cross-ruling. Therefore, the cutting mechanism of abrasives is greatly different from that in ordinary ELID grinding, which not only increases the machining efficiency but also improves the surface machining quality considerably [12].

When analyzing the tallest contour on the workpiece surface, superposition and interleaving between the adjacent grits and workpiece surface must be considered. In Fig. 3, the (k_c) function is introduced to represent the effect and can be expressed as

$$k_c = \frac{\eta_1 \cdot f_a^{\zeta_3}}{f^{\zeta_1}\cdot A^{\zeta_2}}, \tag{11}$$

where η_1, ζ_1, ζ_2, ζ_3 are the correlation coefficients and indexes for measuring the level of correlation between k_c and these variables.

2.3 Additional effects of ELID

In ELID grinding, the dressing of the diamond grinding wheel is performed through metal bond electrolysis to ensure the sharpness of the abrasive grains and obtain an online dressing of the grinding wheel. This process affects the surface topography of the grinding wheel, actual grinding depth, and surface quality of the workpiece. Analysis of the actual grinding depth is therefore important, when the effect of ELID is considered, as shown in Fig. 4.

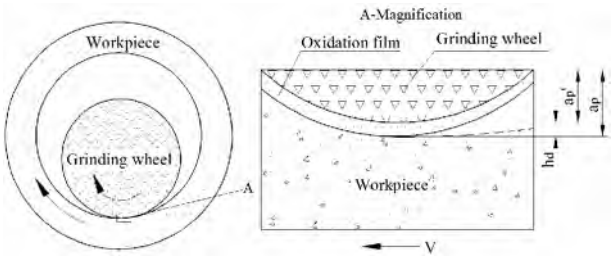

Fig. 4. Electrolysis in ELID grinding.

In Fig. 4, a layer of the oxide film on the grinding wheel can be observed because of ELID. The oxide film exhibits high elastic distortion and thus can grind and polish the workpiece surface, thereby improving surface quality and machining precision. The actual grinding depth (a_p') is the difference between nominal grinding depth (a_p) and thickness of the oxide film (h_d). The oxide film is dynamically balanced by electrolysis and scraping. By Faraday's law of electrolysis, h_d can be expressed as [13]

$$h_d = \eta_2 \frac{M\cdot I\cdot D}{z\cdot F\cdot\rho\cdot A_a} = \frac{\eta_2\cdot M\cdot D\cdot U\cdot A_c}{z\cdot F\cdot\rho\cdot A_a(\rho_e\cdot h_e+\rho_f\cdot h)}, \tag{12}$$

where η_2 is the current efficiency, M is the molecular weight of the metal bond, D is the duty ratio, U is the electrode voltage, A_c is the effective cathode area, z is the valence of metallic element, F is the Faraday's constant, ρ is the density of metal bond, A_a is the effective conducting area at the anode, ρ_e is the electrolyte resistivity, h_e is the inter-electrode gap, ρ_f is the oxidation resistivity, and h is the thickness of the oxide film.

Therefore, the actual grinding depth (a_p') can be expressed as follows:

$$a_p' = a_p - \frac{\eta_2\cdot M\cdot D\cdot U\cdot A_c}{z\cdot F\cdot\rho\cdot A_a(\rho_e\cdot h_e+\rho_f\cdot h)}. \tag{13}$$

2.4 Mathematics model on surface roughness

Using the analysis above, we plug the mathematical expressions of the influencing factors added into Eq. (9), namely, the effects of ultrasonic vibration on adjacent abrasive grits and ELID on the actual grinding depth. Finally, the mathematical model of the surface roughness on the actual ultrasonic vibration-assisted ELID grinding (R_z) is obtained.

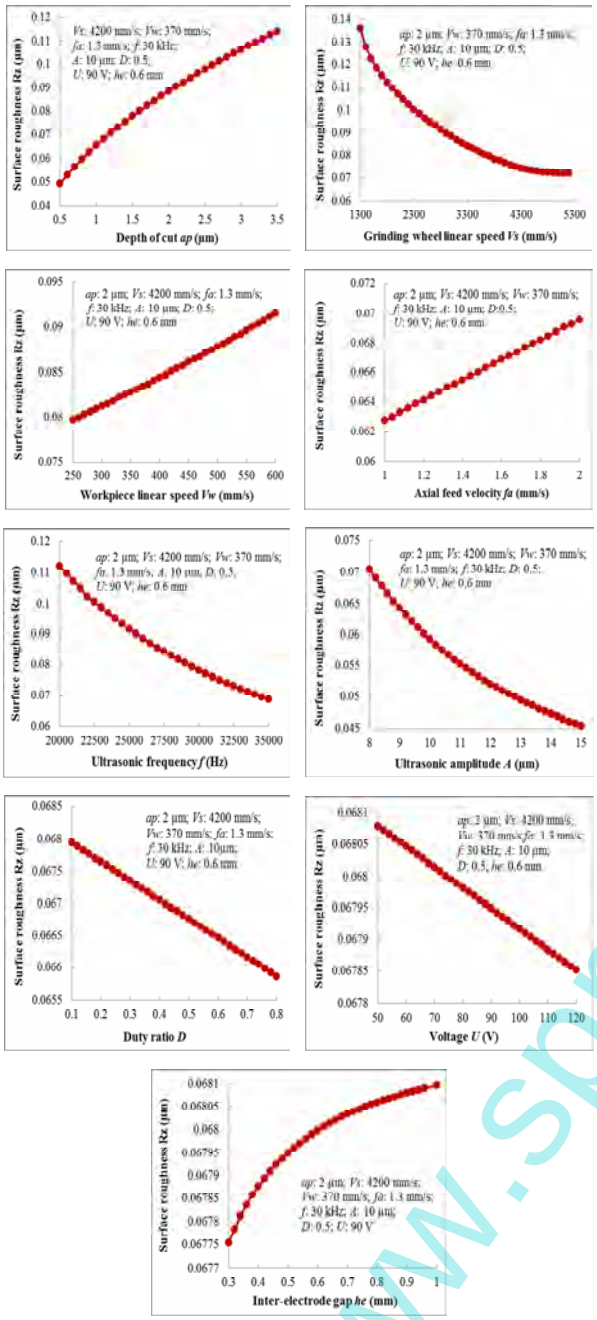

Fig. 5. R_z under different parameters.

$$R_z = \sqrt{2}\cdot\sqrt[3]{\frac{\pi}{6V_g}}\cdot\frac{\eta_1\cdot f_a^{\zeta_3}\cdot d_{g_{avg}}}{f^{\zeta_1}\cdot A^{\zeta_2}\cdot V_s}\cdot\sqrt{a_p'\cdot\left(\frac{R_w-R_s}{R_s\cdot R_w}\right)\cdot\{(R_w+a_p')^2+[\frac{R_w\cdot f_a}{V_s-V_w}+2\cdot A\cdot\pi\cdot f\cdot\frac{R_w}{V_s-V_w}]^2\}} \quad (14)$$

where $a_p' = a_p - \dfrac{\eta_2\cdot M\cdot D\cdot U\cdot A_c}{z\cdot F\cdot\rho\cdot A_a(\rho_e\cdot h_e+\rho_f\cdot h)}$.

As shown in Eq. (14), the actual grinding depth in ultrasonic vibration-assisted ELID grinding is lesser than that in ordinary ELID grinding at same conditions. R_z is determined by grinding wheel, ultrasonic, ELID electrical, and grinding parameters. Under different parameters, the changes in maximum height (R_z) are analyzed using MATLAB. The results are shown in Fig. 5.

The surface roughness increases with the increase in cut depth, workpiece linear speed, axial feed velocity, and inter-electrode gap, whereas it decreases with the increase of grinding wheel linear speed, ultrasonic frequency, ultrasonic amplitude, duty ratio, and voltage. In addition, the degrees of surface roughness changes of the parameters are different from one another. The differences are evident among cut depth, grinding wheel linear speed, ultrasonic frequency, and ultrasonic amplitude. Therefore, combined with additional ultrasonic vibration and ELID, the prediction of the surface quality will be more accurate than that in ordinary ELID grinding or ultrasonic vibration-assisted grinding. In this study, because of the limitations in time and experimental conditions, a part of the surface roughness model (R_z) will be investigated to determine the influence of grinding parameters on surface quality.

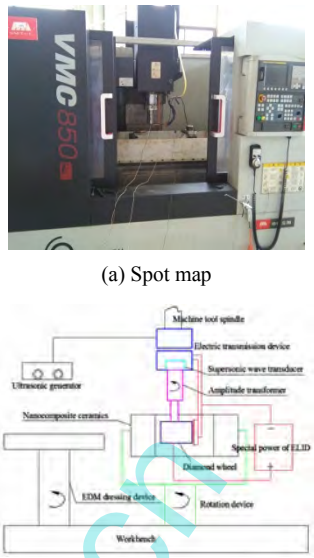

(a) Spot map

(b) Structure diagram of installed equipment

Fig. 6. Test system of ultrasonic vibration-assisted ELID grinding.

3. Experimental conditions

Experiments were conducted on the modified machining center VMC850E, as shown in Fig. 6(a). The electron discharge machining dressing device was installed on the left side of the table, and the rotating device of specimen was positioned on the right side. The electrolytic sharp device was placed above the rotating device and was marked in red in Fig. 6(b). The ultrasonic vibration system was installed on the machining center spindle, which was composed of the electric transmission device, amplitude transformer, and diamond grain. Relevant software and equipment were then integrated into this system.

Table 1. Specific parameters of diamond wheel and ELID.

Object	Parameters	Value
Diamond wheel	Outside diameter	25 mm
	Height	17 mm
	Grain size	280 #
	Concentration	100 %
	Average abrasive particle size	45 microns
ELID	Voltage	90 V
	Inter-electrode gap	1 mm
	Duty ratio	50 %
	Ultrasonic amplitude	8.2 μm
	Ultrasonic frequency	35 kHz

Table 2. Grinding parameters.

Ordinal	V_s (m/s)	V_w (m/s)	f_a (mm/min)	a_p (μm)
1	4.2	0.37	80	2
2	1.3, 2.6, 4.2, 5.2	0.37	80	2
3	4.2	0.28, 0.37, 0.43, 0.50	80	2
4	4.2	0.37	60, 80, 100, 120	2
5	4.2	0.37	80	1, 2, 3, 3.5

Nano-zirconia-toughened alumina nanocomposite ceramic was selected as the research object. The specimens were produced by Jiaozuo Micro-nana Precision Ceramic Production Company through hot isostatic pressing sintering, with maximum sintering temperature at 1640 °C. The machining tool was produced by Zhengzhou Research Institute for Abrasives & Grinding Co. Ltd. The specific parameters of diamond wheel and ELID are shown in Table 1.

Contrastive analysis was used to compare the results, and the absence or presence of ultrasound treatment was used to control the experiment. When the ultrasonic generator was open, the ultrasonic vibration-aided acoustic system started to work. At this time, the experiment was ultrasonic vibration-assisted ELID grinding. Otherwise, it was considered an ordinary ELID grinding experiment. In addition, these experiments using the two methods were researched by single factor experiments. According to the actual test condition and the selection of grinding parameters in the "JIXIE JIAGONG SHIYONG SHOUCE" [14], the grinding parameters selected are those shown in Table 2.

The appropriate measuring equipment is shown in Fig. 7. British Taylor Hobson's contactless Talysurf CCI6000 three-dimensional white light interference surface contour graph is shown in Fig. 7(a), with the arithmetical mean deviation (R_a) and the maximum height (R_z) of the workpiece profile as the measurement indexes. A scanning probe microscope (CSPM-2000) was used to observe the surface microstructure of the samples (Fig. 7(b)). The measurements must be on three points and distributed evenly on each specimen. The average of these data was considered as the final test result.

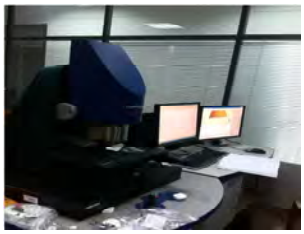

(a) Scanning white-light interfereo-metry profilometer

(b) Scanning probe microscope

Fig. 7. Relevant measuring apparatus.

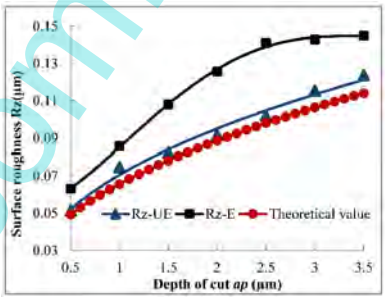

Fig. 8. Effect of grinding depth on surface roughness.

4. Experimental results and discussion

4.1 Effect of grinding depth on surface quality

Change in the surface roughness due to the increase in the grinding depths in ultrasonic vibration-assisted ELID grinding (UE) and ordinary ELID grinding (E) are shown in Fig. 8.

As shown in Fig. 8, the results fit well with experiment data, especially in the ultrasonic vibration-assisted ELID grinding. Moreover, surface roughness significantly increases with the increase of grinding depth, whether under ultrasonic vibration-assisted ELID grinding or under ordinary ELID grinding. The reason for this effect is that when the grinding depth increases, the extrusion resistance between the grinding wheel and the workpiece increases, and the depths of abrasive cutting and cutting groove on the workpiece surface increase. In terms of indentation fracture mechanics, the increasing extrusion resistance can expand the cracks further. Thus, large ceramic materials are subsequently removed, the surface becomes increasingly uneven, and the surface roughness increases. Fig. 8 also indicates that the grinding surface quality under ultrasonic vibration-assisted ELID grinding is better than that under ordinary ELID grinding. In addition, the former exhibit improved range of ductile machining, as indicated in the SEM images of the ultrasonic vibration-assisted ELID grinding (Fig. 9).

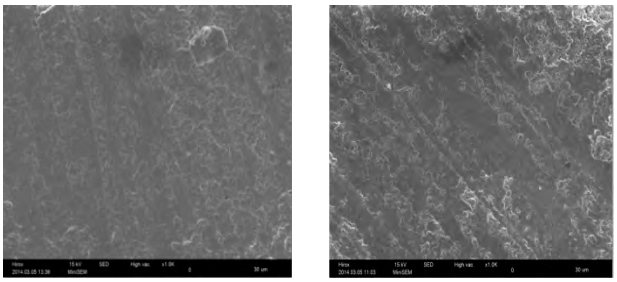

1 μm

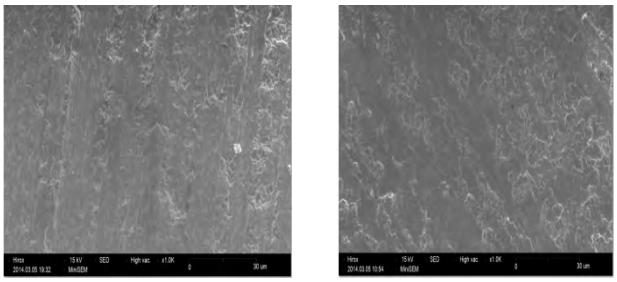

2 μm

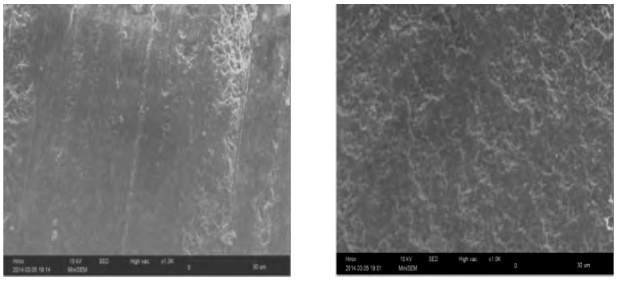

3 μm

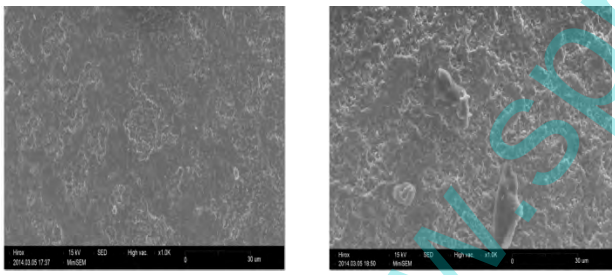

3.5 μm

(a) Ultrasonic vibration-assisted ELID grinding (b) Ordinary ELID grinding

Fig. 9. SEM photos of specimens under different grinding depths.

4.2 Effect of other grinding parameters on surface roughness

A slight difference was observed in the SEM images among the grinding parameters. Thus, a general quantitative analysis of the surface roughness of workpieces under ultrasonic vibration-assisted ELID grinding and ordinary ELID grinding was conducted.

As shown in Fig. 10, the experimental data basically coincides with the theoretical analysis in grinding wheel linear speed, workpiece linear speed, or axial feed velocity. However, a clear difference between theoretical and experimental results is observed. The theoretical analysis is merely scratched the large factors and disregarded the less important factors. Moreover, the large factors were described using mathematical formulas, which cannot fully express all the characteristics of these factors. Therefore, the theoretical analysis was only applicable in ideal scenario, and it cannot completely represent realistic situations. Nevertheless, it can capture the main contradiction. Furthermore, we can attain a more comprehensive understanding of the ultrasonic vibration-assisted ELID machining process and its significance in actual process.

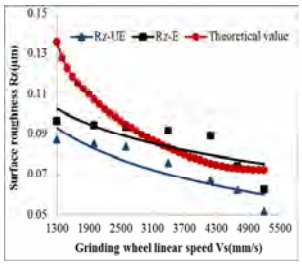

(a) Grinding wheel linear speed

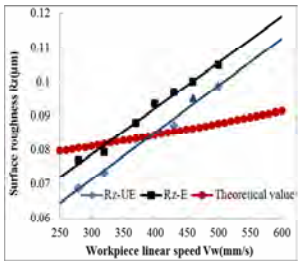

(b) Workpiece linear speed

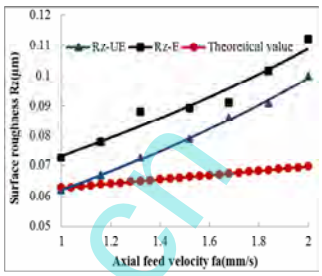

(c) Axial feed velocity

Fig. 10. Effect of other grinding parameters on surface roughness.

The surface roughness in the two methods showed an increasing trend wherein linear speed of the grinding wheel decreases and linear speed and axial feed velocity of the workpiece increse. Moreover, under certain conditions, the surface roughness under ultrasonic vibration-assisted ELID grinding is lower than that under ordinary ELID grinding. In addition, the changes in surface roughness in the former are not evident. These conditions are caused in part by small grinding depth under ultrasonic vibration-assisted ELID grinding; moreover, the scratching depth on the workpiece is reduced, because the ultrasonic vibration trajectory of the abrasive particles increase the interference among the abrasive particles, and this effect influences the abrading workpieces [15].

5. Conclusions

(1) In this study, the interaction between the grits and workpiece surface in ultrasonic vibration-assisted ELID grinding was described, and the surface roughness (R_z) model was developed. The mathematics model on surface roughness is important in forming nano-composite ceramics.

(2) Under the same condition, the surface quality under ultrasonic vibration-assisted ELID grinding was higher than that under ordinary ELID grinding, and the total variation was not apparent. Moreover, the ultrasonic vibration-assisted ELID grinding can determine a wide range of ductility processing, as indicated in previous research results [11]. This finding shows that ultrasonic vibration-assisted ELID grinding is more suitable for precision machining of nano-composite ceramics, compared with ordinary ELID grinding.

Acknowledgment

The authors would like to acknowledge the National Science Foundation of China (Contract No. 51175153 and 51475148), Project supported by the Fostering Foundation of Henan Polytechnic University for the Excellent Ph.D. Dissertation, for their financial support. We would also like to give our sincere thanks to the reviewers for their professional suggestions.

Nomenclature

A : Ultrasonic frequency
A_a : Effective conducting area at the anode
A_c : Effective cathode area
a_p : Nominal grinding depth
a_p' : Actual grinding depth
C_s : Concentration of abrasive grinding wheel
D : Duty ratio
d_{gavg} : Average diameter of abrasive particle
F : Faraday's constant
f : Ultrasonic amplitude
f_a : Axial feed velocity
h : Oxidation resistivity
h_d : Thickness of oxide film
h_e : Inter-electrode gap
k_c : Function to represent the ultrasonic effect
M : Molecular weight of metal bond
R_s : Radius of grinding wheel
R_w : Radius of workpiece
R_z : Surface roughness on the actual ultrasonic vibration-assisted ELID grinding
R_z' : Surface roughness formed by single diamond grit under ultrasonic vibration
r_s : Radius of diamond grinding wheel grain
U : Electrode voltage
V_g : Volume fraction of abrasive in grind wheel
V_f : Feed speed of work table
V_s : Speed of grinding wheel
V_w : Speed of grinding wheel
z : Valence of metallic element
α : Angle of abrasive corresponding to the corner of workpiece
β : Angle of abrasive corresponding to the corner of grinding wheel
ζ_1 : Correlation coefficient
ζ_2 : Correlation coefficient
ζ_3 : Correlation coefficient
η_1 : Correlation coefficient
η_2 : Current efficiency
θ : Angle of trajectory with its corresponding string
ρ : Density of metal bond
ρ_e : Electrolyte resistivity
ρ_f : Oxidation resistivity
φ : Initial angle of ultrasonic vibration
Δ : Internal space between two adjacent grits

References

[1] K. R. Nemade, R. V. Barde and S. A. Waghuley, Photocatalytic study of alumina-zirconia ceramic nanocomposite synthesized by spray pyrolysis, *Ceramics International*, 41 (2015) 4836-4840.
[2] S. Farhan, R. Wang and H. Jiang, A novel method for the processing of carbon foam containing in situ grown nanomaterials and silicon nanowires, *Materials Letters*, 159 (2015) 439-442.
[3] S. D. Yoon, H. S. Byun and Y. H. Yun, Characterization and photocatalytic properties of ceramics TiO_2 nanocomposites, *Ceramics International*, 41 (2015) 8241-8246.
[4] M. M. Islama, K. A. Senthil, S. Balakumar, H. S. Lim and M. Rahman, Characterization of ELID grinding process for machining silicon wafers, *Journal of Materials Processing Technology*, 198 (2008) 281-290.
[5] S. H. Yin, H. Ohmori, Y. T. Dai, Y. Uehara, F. J. Chen and H. N. Tang, ELID grinding characteristics of glass-ceramic materials, *International Journal of Machine Tools & Manufacture*, 49 (2009) 333-338.
[6] D. Wang, S. Takeo and Y. Hitomi, Study of magnetic field assisted mechanochemical polishing process for inner surface of Si_3N_4 ceramic components finishing characteristics under wet finishing using distilled water, *International Journal of Machine Tools & Manufacture*, 44 (2004) 1547-1553.
[7] G. F. Gao, B. Zhao, D. H. Xiang and Q. H. Kong, Research on the surface characteristics in ultrasonic grinding nano-zirconia ceramics, *Journal of Materials Processing Technology*, 209 (2009) 32-37.
[8] Z. Ali, T. Taghi and A. Javad, Energy aspects and workpiece surface characteristics in ultrasonic-assisted cylindrical grinding of alumina-zirconia ceramics, *International Journal of Machine Tools & Manufacture*, 90 (2015) 16-28.
[9] M. Novak, H. Kasuga and H. Ohmori, Differences at the surface roughness by the ELID and grinding technology, *Manufacturing Technology*, 13 (2013) 210-215.
[10] B. Zhao, L. Z. Kong and C. Y. Zhao, Study on the node position of stepped horn used for power ultrasonic grinding, *Key Engineering Materials*, 455 (2011) 103-109.
[11] F. Chen, B. Zhao, X. F. Jia and X. B. Wang, Material removal rate for nanocomposite ceramics in ultrasound-

aided electrolytic in process dressing, *Part C: J Mechanical Engineering Science* (2016) 1-12.
[12] K. Katahira, Y. Watanabe, H. Ohmori and T. Kato, ELID grinding and tribological characteristics of TiAlN film, *International Journal of Machine Tools and Manufacture*, 42 (2002) 1307-1313.
[13] Z. Liu, B. Zhao, Y. Y. Zheng and P. Y. Pian, Simulation on mechanism of ceramic removal by ultrasonic ELID composite grinding, *Ordnance Material Science and Engineering*, 37 (2014) 27-31 (In Chinese).
[14] Z. Y. Xia and N. W. Zhang, *Jixie Jiagong Shiyong Shouce*, Hefei: Anhui science and technology publishing house, China (2008).
[15] S. H. Alavi and S. P. Harimkar, Evolution of geometric and quality features during ultrasonic vibration-assisted continuous wave laser surface drilling, *Journal of Materials Processing Technology*, 232 (2016) 52-62.

Bo Zhao received his Ph.D. from the School of Mechanical Engineering in Shanghai Jiao Tong University, Shanghai, China, in 1999. He currently works at Henan Polytechnic University. His research interests include advanced manufacturing technology and precision machining theory and equipment.

Fan Chen is a Ph.D. student at the School of Mechanical and Power Engineering in Henan Polytechnic University of Jiaozuo, China. Her current research interests are precision and super precision manufacturing technology, especially those applied in sultrasonic vibration-assisted machining.